This article has been accepted for publication in a future issue of this journal, but has not been fully edited. Content may change prior to final publication. Citation information: DOI 10.1109/TNB.2022.3170562, IEEE Transactions on NanoBioscience

Motility resilience of molecular shuttles against defective motors

Samuel Macharia Kang'iri and Takahiro Nitta*, *Member, IEEE*

***Abstract*—Myosin and kinesin are biomolecular motors found in living cells. By propelling their associated cytoskeletal filaments, these biomolecular motors facilitate force generation and material transport in the cells. When extracted, the biomolecular motors are promising candidates for *in vitro* applications such as biosensor devices, on account of their high operating efficiency and nanoscale size. However, during integration into these devices, some of the motors become defective due to unfavorable adhesion to the substrate surface. These defective motors inhibit the motility of the cytoskeletal filaments which make up the molecular shuttles used in the devices. Difficulties in controlling the fraction of active and defective motors in experiments discourage systematic studies concerning the resilience of the molecular shuttle motility against the impedance of defective motors. Here, we used mathematical modelling to systematically examine the resilience of the propulsion by these molecular shuttles against the impedance of the defective motors. The model showed that the fraction of active motors on the substrate is the essential factor determining the resilience of the molecular shuttle motility. Approximately 40% of active kinesin or 80% of active myosin motors are required to constitute continuous gliding of molecular shuttles in their respective substrates. The simplicity of the mathematical model in describing motility behavior offers utility in elucidating the mechanisms of the motility resilience of molecular shuttles.**

***Index Terms*—Biomedical engineering, bionanotechnology, biophysics, biosensors, microelectromechanical systems, nanobioscience**

I. Introduction

Motor proteins, such as myosin and kinesin, are biomolecular motors that actuate movement in living cells. Myosin and kinesin are typical biomolecular motors ubiquitous in the cells. Through repeated mechanochemical cycles of hydrolysis of adenosine triphosphate (ATP), myosin and kinesin attach to and detach from the actin and microtubule filaments, respectively, to constitute movements. The actin and myosin pairs produce contraction movements in muscle cells, while microtubule and kinesin pairs contribute to intracellular material transport. These biomolecular motors can be harnessed *in vitro* for nano- and microscale synthetic applications [1][2][3][4][5][6][7], which include biosensors [8][9][10][11][12], biocomputers [13], and molecular communication devices [14][15]. In such applications, biomolecular motors drive their associated cargo-loaded cytoskeletal filaments, forming a molecular shuttle system. Owing to their small size and high energy conversion efficiency, molecular shuttle systems are indispensable to applications involving active transport.

The two biomolecular motors often utilized for molecular shuttles, kinesin and myosin, have distinct properties. On the one hand, microtubule-based molecular shuttles move over kinesin-coated surfaces with speeds of 0.5-1 μm/s along rather straight trajectories with the path persistence length of 0.1 mm [16][17]. On the other hand, actin-based molecular shuttles move over myosin-coated surfaces with speeds of 2-7 μm/s along rather twisted trajectories with the path persistence length of 0.01 mm [18][19]. These differences affect the performance of devices that utilize molecular shuttles [20][21]. The higher gliding speed of actin-based molecular shuttles is preferable for fast detection and computation, in contrast to the lower microtubule-based gliding speed. While microtubule-based molecular shuttles are easier to guide with tracks made by conventional photolithography [22][23], more sophisticated electron lithography is needed to make actin-based guiding tracks [24].

Another factor to consider is resilience of motility against defective motors. When biomolecular motors are adhering to the substrate surface, some of them become defective due to

Samuel Macharia Kang'iri is with the Department of Electronics and Information Systems Engineering, Gifu University, Gifu, 501-1193 Japan (x3914101@edu.gifu-u.ac.jp), on leave from Department of Mechatronics Engineering, Dedan Kimathi University of Technology, Nyeri, 657-10100 Kenya (samuel.macharia@dkut.ac.ke).

*Takahiro Nitta is with the Applied Physics Course, Faculty of Engineering, Gifu University, Gifu, 501-1193 Japan (nittat@gifu-u.ac.jp).

unfavorable interactions between the surface and the biomolecular motors. Defective motors do not hydrolyze ATP and may only bind to their associated filaments. Thus, defective motors do not translate them, and these motors act as impedance to propulsion of molecular shuttles. The impedances by defective motors lead to slowing down, fishtailing [25], swirling [25], and even halting of molecular shuttles. In biophysical studies, to achieve smooth movements of cytoskeletal filaments gliding over biomolecular motors in *in vitro* motility assay, defective motors have to be carefully removed prior to observation of movement, and the surfaces should be passivated to prevent "non-ideal" adhesion of biomolecular motors to the surface leading to denaturization, especially for the actin and myosin system [26]. In applications, polymer materials such as photoresists are used for substrates, and these polymers facilitate denaturing of motor proteins [27], which makes motility resilience of molecular shuttles of practical importance.

Understanding the motility resilience of both microtubule-based and actin-based molecular shuttles presents important practical insights in using molecular shuttles, as well as biophysical perspectives of biomolecular motors and cytoskeletal filaments. Nevertheless, systematic experimental investigations are hampered by difficulties in controlling the precise amount of defective motors on substrate surfaces. Computer simulations are useful in offering systematic means for investigating this problem but at extensive computational cost. Alternatively, a mathematical model capturing the essence of underlying mechanisms would be a complementary approach with an advantage of providing a simplified view of these mechanisms. In this study, we investigated the resilience of motility of molecular shuttles driven by biomolecular motors against the presence of defective motors. The simplicity of the mathematical model makes it easy to gain insights into the motility resilience of molecular shuttles.

This manuscript is an extended version of our conference paper for 13th EAI International Conference on Bio-inspired Information and Communications Technologies (BICT2021) conference paper [28]. In the conference paper, we showed how a mathematical model could be used to predict the gliding speed of the actin-based molecular shuttles against defective motors. In this study, we have extended the application of the model to the microtubule-based molecular shuttles as well, which enabled comparisons between the two types of molecular shuttles with distinct biophysical properties.

II. Mathematical Modelling

To predict the translocation of cytoskeletal filaments under impedance by defective motors, we developed a 1D mathematical model based on a previous study [29]. Our 1D model assumes that cytoskeletal filaments are propelled by active motors acting against impedance generated by defective ones (Fig. 1). The gliding speed (v) is assumed to depend on the average force acting on each active motor (f):

$$v = \begin{cases} v_{max}\left(1 - \frac{f}{f_{stall}}\right) & (f_{stall} \le f \le 0) \\ 0 & (f < f_{stall}) \end{cases} \quad (1)$$

where v_{max} is the maximum speed of the translocation of cytoskeletal filaments, and f_{stall} is the stall force of the associated biomolecular motors. Although (1) results from cyclic binding and unbinding of active motors to cytoskeletal filaments, for simplicity, spontaneous dissociations of active motors are not explicitly included. This treatment can be validated provided that the motor density is high enough such that the spontaneous detachments of cytoskeletal filaments are rare [30].

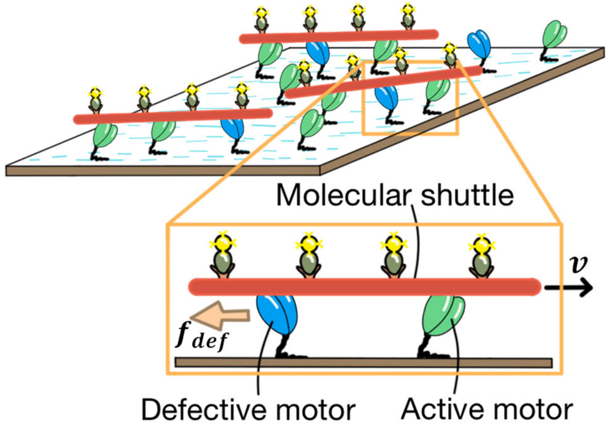

Fig. 1. A schematic drawing of molecular shuttles gliding over biomolecular motors in the presence of defective motors.

The acting force, f, is assumed to be exerted by the defective motors. During the cytoskeletal filament translocations, defective motors undergo repeated cycles of associations with cytoskeletal filaments, elongation and then dissociations from the cytoskeletal filaments (Fig. 2). When the cytoskeletal filaments approach closely, the defective motors bind to these filaments with a rate of $1/\tau_1$. Once bound, defective motors are gradually stretched by the cytoskeletal filament translocations, building up tension that impedes further cytoskeletal filament translocations. When the tensions reach the rupture force of the biomolecular motors, f_{rupt}, the defective motors dissociate from the cytoskeletal filaments. For simplicity, spontaneous dissociations of defective motors from cytoskeletal filaments were neglected here. It is assumed that cytoskeletal filaments move with a constant gliding speed depending on the acting impedance, then the durations, τ_2, that the defective motors remain bound to cytoskeletal filaments depend on the cytoskeletal filament speeds and they are given by $\tau_2 = -f_{rupt}/kv$, where k is the spring constant of the defective motors. Thus, the time-averaged force generated by a defective motor, $\overline{f_{def}}$, is given by:

$$\overline{f_{def}} = \frac{1}{\tau_1+\tau_2}\int_0^{\tau_1+\tau_2} f_{def}\,dt. \quad (2)$$

Guided by Fig. 2, the integral in (2) can be evaluated, leading to (3).

$$\overline{f_{def}} = \frac{f_{rupt}}{2\left(1-k v \tau_1/f_{rupt}\right)} \quad (3)$$

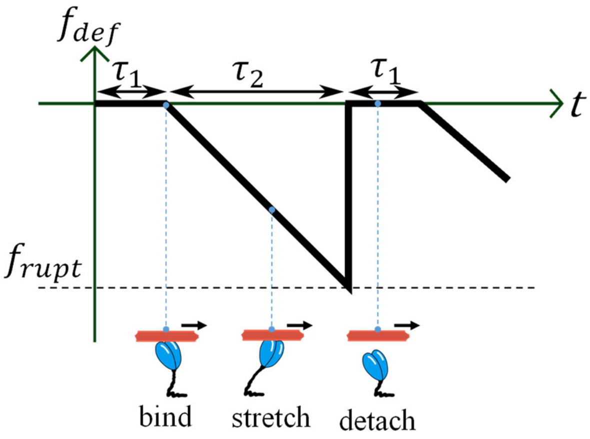

Fig. 2. A schematic representation of the time evolution of the force generated by a defective motor.

Since the number of the active motors binding to cytoskeletal filaments with the length of L is $\rho_a L$ and that of the defective ones $\rho_d L$, where ρ_a and ρ_d are the line densities of active and defective motors, respectively, the impedance per active motor is given as follows:

$$f_{imp} = \frac{\rho_d}{\rho_a} \frac{f_{rupt}}{2\left(1-k v \tau_1/f_{rupt}\right)}. \quad (4)$$

From (1), once the impedance is given, the gliding speed of cytoskeletal filaments can be calculated. On the other hand, to determine the impedance from (4), the gliding speeds of cytoskeletal filaments are needed. Thus, to obtain the cytoskeletal filament gliding speed, we need to solve (1) and (4) self-consistently. The gliding speed can be obtained from graphs at the intersection of (1) and (4) (Fig. 3), or analytically as in (5):

$$v = \frac{f_{rupt}}{2k\tau_1}\left[\left(1+\frac{k v_{max}\tau_1}{f_{rupt}}\right) + \sqrt{\left(1+\frac{k v_{max}\tau_1}{f_{rupt}}\right)^2 + \frac{4 k v_{max}\tau_1}{f_{rupt}}\left(1-\frac{f_{rupt}}{2 f_{stall}}\frac{\rho_d}{\rho_a}\right)}\right], \quad (5a)$$

$$v = \frac{f_{rupt}}{2k\tau_1}\left[\left(1+\frac{k v_{max}\tau_1}{f_{rupt}}\right) - \sqrt{\left(1+\frac{k v_{max}\tau_1}{f_{rupt}}\right)^2 + \frac{4 k v_{max}\tau_1}{f_{rupt}}\left(1-\frac{f_{rupt}}{2 f_{stall}}\frac{\rho_d}{\rho_a}\right)}\right] \quad (5b)$$

The solution (5b) is unstable as is shown in the Sec. III.

The parameters used in this study are listed in Table 1. The gliding speed, v, is a function of ρ_d/ρ_a. To make comparisons with experiments [31][27], we also use active motor ratio, r, given by (7):

$$r = \frac{\rho_a}{\rho_a+\rho_d}. \quad (7)$$

TABLE 1: PARAMETERS USED

Parameter	Description	Microtubule-kinesin	Actin-myosin
v_{max}	Maximum gliding speed	0.8 µm/s [32]	7 µm/s [33]
f_{stall}	Stall force	-5 pN [32]	-0.4 pN [34][35]
f_{rupt}	Rupture force	-7 pN [36]	-9.2 pN [37]
k	Spring constant	100 pN/µm [38]	300 pN/µm [39]
τ_1	Binding period	0.2 s [40]	0.025 s [39]

III. MODEL PREDICTIONS

In this section, we obtain generic predictions of the mathematical model. These generic predictions are applied to microtubule-based and actin-based molecular shuttles in Sec. IV.

It is evident from Fig. 3(a) that when the slope of (4) is larger than that of (1), there is only one solution of (5a) despite the value of ρ_d/ρ_a. On increasing ρ_d/ρ_a (the red curves #1 to #4 in Fig. 3(a)), the gliding speed continuously decreases until $v = 0$ at $\rho_d/\rho_a = 2 f_{stall}/f_{rupt}$ (Fig. 3(b)). In other words, the stationary-motile transition is continuous. The slope of (4) when $\rho_d/\rho_a = 2 f_{stall}/f_{rupt}$ is given by $2 f_{rupt}/k\tau_1 f_{stall}$. The slope of (1) is $-v_{max}/f_{stall}$. Thus, the condition is obtained that the continuous transition occurs at $-k\tau_1 v_{max}/2f_{rupt} \leq 1$.

In the event that $-k\tau_1 v_{max}/2f_{rupt} > 1$, that is, the slope of (1) is steeper than that of (4), depending on ρ_d/ρ_a, there are three cases. Case 1: at small ρ_d/ρ_a (the red curve #1 in Fig. 3(c)), there is only one solution of (5a). Case 2: at intermediate ρ_d/ρ_a (the red curve #2 in Fig. 3(c)), there are two solutions of (5a) and (5b). These two solutions coincide at the critical value of ρ_d/ρ_a (the red curve #3 in Fig. 3(c)) given by

$$\left(\frac{\rho_d}{\rho_a}\right)_c = \frac{2 f_{stall}}{f_{rupt}}\left[1-\frac{f_{rupt}}{4 k v_{max}\tau_1}\left(1+\frac{k v_{max}\tau_1}{f_{rupt}}\right)^2\right]. \quad (6)$$

Case 3: above the critical value (the red curve #4 in Fig. 3(c)), there is no motile solution and only a stationary solution is obtained.

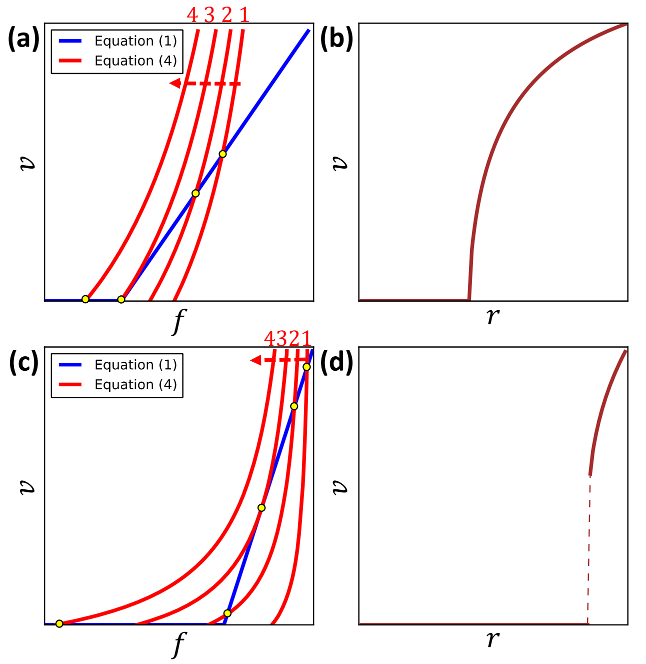

Fig. 3. (a, c) Schematic plots of the gliding speeds as functions of impedance given by (4) with various active motor ratios, overlaid with the $f-v$ relation of (1). (b, d) Gliding speeds, v, as function of active motor ratio, r. (a) and (b): continuous, (c) and (d): discontinuous. The arrows in (a) and (c) point to the direction of increasing ρ_d/ρ_a.

When there are two solutions at intermediate ρ_d/ρ_a, (5a) is stable while (5b) is unstable as described below. First, we consider fluctuations in the gliding speed around the solution with a higher gliding speed, (5a). Although we have so far only discussed averaged behavior, the cytoskeletal filament gliding speed may fluctuate about the average with occasional increases or decreases. For example, for the high speed solution (Fig. 4 (a)), if the cytoskeletal filament speed increases (the yellow arrow #1 in Fig. 4(a)), the impedance coinciding with the new higher speed is larger, hence causing the filament speed to decelerate back to its original gliding speed (the yellow arrow #2 in Fig. 4(a)). If, on vice versa, the cytoskeletal filament speed at this high speed solution decreases due to fluctuation, impedance will drop, causing the filament to accelerate back to its original gliding speed. The high speed solution is hence a stable solution. Conversely, for the low speed solution by (5b) that is plotted in Fig. 4(b), when a cytoskeletal filament happens to be accelerated by fluctuation (the yellow arrow #1 in Fig. 4(b)), the impedance at this new higher speed is smaller, leading to the further acceleration of the cytoskeletal filament (the yellow arrow #2 in Fig. 4(b)), showing that the solution is unstable. Taking the stable solutions, we obtain the gliding speed as a function of ρ_d/ρ_a or r. The gliding speed is independent of the length of the cytoskeletal filament, and ρ_d/ρ_a is the single parameter that determines the gliding speed.

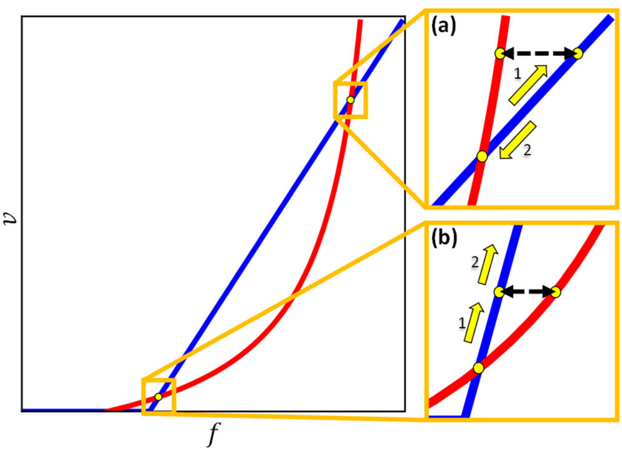

Fig. 4. Schematic representations of stability analysis of steady state solutions of molecular shuttle gliding speed. (a) Stability analysis of the steady state solution with high gliding speed, a stable solution. (b) Stability analysis of the steady state solution with low gliding speed, an unstable solution. The red curve represents (4) and the blue line represents (1). Yellow arrows with numbers represent increasing or decreasing speed. The black arrows indicate a shift in impedance at that point.

Continuity of the stationary-motile transition can have significant effects on the behavior of cytoskeletal filaments placed on surfaces close to the critical ratio of (6). In experiments, there is always some inhomogeneity of densities of active and defective biomolecular motors. Such inhomogeneity may cause inhomogeneity of motility within a cytoskeletal filament. Some parts of the cytoskeletal filament may be in regions with slightly lower ρ_d/ρ_a than its critical value of (6), hence they may be propelled, while the other parts may be in regions with slightly higher ρ_d/ρ_a than its critical value, and hence they may be stationary. The inhomogeneity in motility may cause undulation and even breaks of cytoskeletal filaments.

IV. Applying Predictions to Microtubule-Kinesin and Actin-Myosin Systems

Here we apply the above generic predictions of the mathematical model to microtubule-based and actin-based molecular shuttles.

For microtubule-based molecular shuttles, using the parameter values listed in Table 1, $-k\tau_1 v_{max}/2f_{rupt} = 1.143$, so that the stationary-motile transition is slightly discontinuous. In Fig. 5, with r of greater than 0.412, there is only one motile solution. With r between 0.372 and 0.412, there are two motile

This article has been accepted for publication in a future issue of this journal, but has not been fully edited. Content may change prior to final publication. Citation information: DOI 10.1109/TNB.2022.3170562, IEEE Transactions on NanoBioscience

solutions. At $r = 0.372$, the two solutions coincide. Below $r = 0.372$, there is only a stationary solution. Fig. 6 shows gliding speed of microtubule-based molecular shuttles for various r. The stationary-motile transition occurs at the active motor ratio of 0.372, which is reasonably close to experiment and simulation results [31].

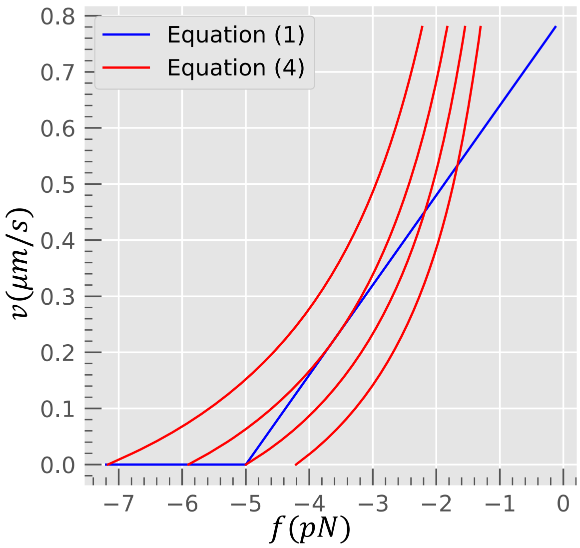

Fig. 5. Plots for microtubule-based molecular shuttles of the gliding speed, v, as a function of impedance given by (4) with various active motor ratios, r (red curves), overlaid with the $f - v$ relation of (1) (blue line). The active motor ratio is 0.328, 0.372, 0.412, and 0.454 from left to right. The critical active motor ratio in this case is 0.372.

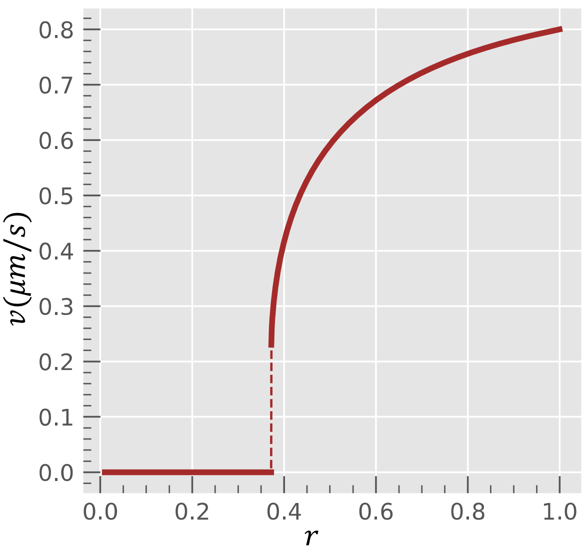

Fig. 6. The microtubule gliding speed, v, as a function of the active motor ratio, r.

For actin-based molecular shuttles, $-k\tau_1 v_{max}/2f_{rupt} = 2.853$, so that the stationary-motile transition is discontinuous (Fig. 7). The gliding of actin filaments can only occur with a rather high active motor ratio of 0.854 or more (Fig. 8). This range of active motor ratio allowing motility is somewhat higher than that obtained in the experiment [27] and reasonably close to that obtained in the simulation [41]. This discrepancy from the experiment can be explained by the surface density of the accessible myosin motors on polymer substrates [41].

A few differences should be noted when comparing actin-based and microtubule-based molecular shuttles. The range of active motor ratio allowing motility is considerably narrower for actin-based molecular shuttle in contrast to that for microtubule-based molecular shuttles. The need for the higher critical active motor ratio for gliding of actin filaments over myosin than for microtubules over kinesin motors is consistent with the fact that more procedures to remove defective heads are needed to achieve consistent gliding for actin-myosin *in vitro* motility assay. The stationary-motile transition occurs abruptly in actin-based molecular shuttles but rather continuously in microtubule-based molecular shuttles. According to the discussion at the end of Sec. III, it appears consistent with the fact that actin filaments often show undulated conformations and break on insufficiently prepared surfaces although flexural rigidities of cytoskeletal filaments also play an important role.

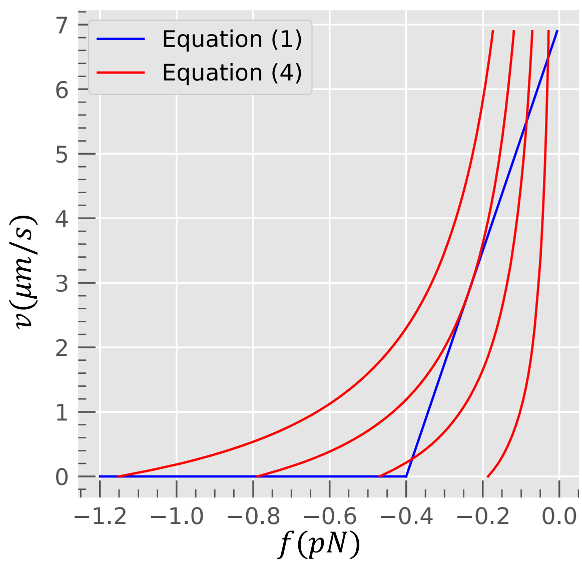

Fig. 7. Plots for actin-based molecular shuttles of the gliding speed, v, as a function of impedance given (4) with various active motor ratios, r (red curves), overlaid with the $f - v$ relation of (1) (blue line). The active motor ratio is 0.800, 0.854,

0.908, and 0.962 from left to right. The critical active motor ratio in this case is 0.854.

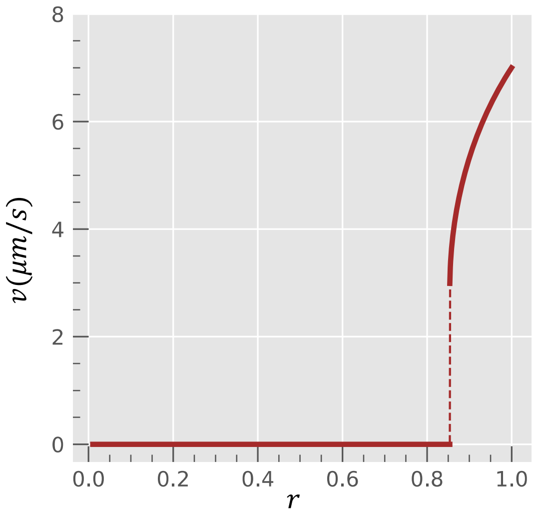

Fig. 8. The actin filament gliding speed, v, as a function of the active motor ratio, r.

V. Conclusions

Our 1D mathematical model showed that the active motor ratio $\rho_a/(\rho_a+\rho_d)$ was the single important factor that influenced motility of molecular shuttles, and that active ratios of more than 40% and 80% were required for continuous gliding movement of microtubules over kinesin motors and for actin filaments over myosin motors, respectively. Our model successively reproduced experimental results and revealed that microtubule-kinesin was more resilient against contamination of defective motors than actin-myosin was.

A shortcoming of this study may be that only 1D movements were considered. This may affect the value of the critical active motor ratio because cytoskeletal filaments gliding over biomolecular motors, in particular actin filaments gliding over myosin motors, can show undulation, which may alter the critical active motor ratio of the stationary-motile transition. The use of computer simulation can offer a complementary approach to this study by dealing with such movements [32][42].

The simplicity of our mathematical model was shown to be useful in elucidating movements. Considering the simplicity of the model, its predictions agreed surprisingly well with previous results of experiments and simulations for both microtubule-kinesin and actin-myosin systems. The agreements can be further explored by using a more realistic relationship between force and speed such as the Hill equation for actin-myosin [43]. However, a drawback would be the complexity of the mathematical expression and the increasing numbers of parameters, which may make it complicated to elucidate the underlying mechanisms. Using Michaelis-Menten kinetics of ATPase activities of active motors and other dependencies of the parameters against biochemical variables, such as ionic strength, this model may be used to extrapolate the biochemical variables of assay conditions. It is desirable to take advantage of the simplicity of the presented model to interpret experimental results and to reduce the parameter space before attempting to run computationally expensive simulations.

References

[1] G. Saper and H. Hess, "Synthetic Systems Powered by Biological Molecular Motors.," *Chem. Rev.*, vol. 120, no. 1, pp. 288–309, Jan. 2020.

[2] G. D. Bachand, N. F. Bouxsein, V. VanDelinder, and M. Bachand, "Biomolecular motors in nanoscale materials, devices, and systems," *WIREs Nanomedicine and Nanobiotechnology*, vol. 6, no. 2, pp. 163–177, Mar. 2014.

[3] A. Agarwal and H. Hess, "Biomolecular motors at the intersection of nanotechnology and polymer science," *Prog. Polym. Sci.*, vol. 35, no. 1–2, pp. 252–277, Jan. 2010.

[4] D. J. G. Bakewell and D. V. Nicolau, "Protein Linear Molecular Motor-Powered Nanodevices," *Aust. J. Chem.*, vol. 60, no. 5, pp. 314–332, May 2007.

[5] T. Korten, A. Månsson, and S. Diez, "Towards the application of cytoskeletal motor proteins in molecular detection and diagnostic devices," *Current Opinion in Biotechnology*, vol. 21, no. 4. Elsevier Current Trends, pp. 477–488, 01-Aug-2010.

[6] A. Månsson, "Translational actomyosin research: Fundamental insights and applications hand in hand," *Journal of Muscle Research and Cell Motility*, vol. 33, no. 3–4. Springer, pp. 219–233, 26-May-2012.

[7] C. Dong and C. Z. Dinu, "Molecular trucks and complementary tracks for bionanotechnological applications," *Current Opinion in Biotechnology*, vol. 24, no. 4. Elsevier Current Trends, pp. 612–619, 01-Aug-2013.

[8] G. D. Bachand, H. Hess, B. Ratna, P. Satir, and V. Vogel, "'Smart dust' biosensors powered by biomolecular motors," *Lab Chip*, vol. 9, no. 12, pp. 1661–1666, 2009.

[9] C. T. Lin, M. T. Kao, K. Kurabayashi, and E. Meyhofer, "Self-contained, biomolecular motor-driven protein sorting and concentrating in an ultrasensitive microfluidic chip," *Nano Lett.*, vol. 8, no. 4, pp. 1041–1046, 2008.

[10] T. Fischer, A. Agarwal, and H. Hess, "A smart dust biosensor powered by kinesin motors," *Nat. Nanotechnol.*, vol. 4, no. 3, pp. 162–166, Mar. 2009.

[11] M. Lard *et al.*, "Ultrafast molecular motor driven nanoseparation and biosensing," *Biosens. Bioelectron.*, vol. 48, pp. 145–152, Oct. 2013.

[12] N. Isozaki, H. Shintaku, H. Kotera, T. L. Hawkins, J. L. Ross, and R. Yokokawa, "Control of molecular shuttles by designing electrical and mechanical properties of microtubules," *Sci. Robot.*, vol. 2, no. 10, p. eaan4882, Sep. 2017.

[13] D. V Nicolau *et al.*, "Parallel computation with molecular-motor-propelled agents in nanofabricated networks," *Proc. Natl. Acad. Sci. U. S. A.*, vol. 113, no. 10, pp. 2591–2596, 2016.

[14] T. Nakano, M. J. Moore, F. Wei, A. V. Vasilakos, and J. Shuai, "Molecular communication and networking: opportunities and challenges.," *IEEE Trans. Nanobioscience*, vol. 11, no. 2, pp. 135–48, Jun. 2012.

[15] N. Farsad, H. B. Yilmaz, A. Eckford, C.-B. Chae, and W. Guo, "A Comprehensive Survey of Recent Advancements in Molecular Communication," *IEEE Commun. Surv. Tutorials*, vol. 18, no. 3, pp. 1887–1919, Oct. 2014.

[16] T. Nitta and H. Hess, "Dispersion in active transport by kinesin-powered molecular shuttles," *Nano Lett.*, vol. 5, no. 7, pp. 1337–1342, Jul. 2005.

[17] M. G. L. Van Den Heuvel, M. P. De Graaff, and C. Dekker, "Microtubule curvatures under perpendicular electric forces reveal a low persistence length," *Proc. Natl. Acad. Sci. U. S. A.*, vol. 105, no. 23, pp. 7941–7946, Jun. 2008.

[18] T. Nitta *et al.*, "Comparing guiding track requirements for myosin-and kinesin-powered molecular shuttles," *Nano Lett.*, vol. 8, no. 8, pp. 2305–2309, 2008.

[19] P. G. Vikhorev, N. N. Vikhoreva, and A. Månsson, "Bending flexibility of actin filaments during motor-induced sliding," *Biophys. J.*, vol. 95, no. 12, pp. 5809–5819, Dec. 2008.

[20] T. Nitta and H. Hess, "Effect of path persistence length of molecular shuttles on two-stage analyte capture in biosensors," *Cell. Mol. Bioeng.*, vol. 6, no. 1, pp. 109–115, 2013.

[21] C. Reuther *et al.*, "Comparison of actin- And microtubule-based motility systems for application in functional nanodevices," *New Journal of Physics*, vol. 23, no. 7. IOP Publishing, p. 075007, 26-Jul-2021.

[22] H. Hess, J. Clemmens, D. Qin, J. Howard, and V. Vogel, "Light-Controlled Molecular Shuttles Made from Motor Proteins Carrying Cargo on Engineered Surfaces," *Nano Lett.*, vol. 1, no. 5, pp. 235–239, May 2001.

[23] Y. Hiratsuka, T. Tada, K. Oiwa, T. Kanayama, and T. Q. P. Uyeda, "Controlling the direction of kinesin-driven microtubule movements along microlithographic tracks," *Biophys. J.*, vol. 81, no. 3, pp. 1555–1561, Sep. 2001.

[24] M. Sundberg *et al.*, "Actin filament guidance on a chip: Toward high-throughput assays and lab-on-a-chip applications," *Langmuir*, vol. 22, no. 17, pp. 7286–7295, 2006.

[25] L. Bourdieu, T. Duke, M. B. Elowitz, D. A. Winkelmann, S. Leibler, and A. Libchaber, "Spiral defects in motility assays: A measure of motor protein force," *Phys. Rev. Lett.*, vol. 75, no. 1, pp. 176–179, 1995.

[26] M. A. Rahman, A. Salhotra, and A. Månsson, "Comparative analysis of widely used methods to remove nonfunctional myosin heads for the in vitro motility assay," *J. Muscle Res. Cell Motil.*, vol. 39, no. 5–6, pp. 175–187, Dec. 2018.

[27] K. L. Hanson *et al.*, "Polymer surface properties control the function of heavy meromyosin in dynamic nanodevices," *Biosens. Bioelectron.*, vol. 93, pp. 305–314, Jul. 2017.

[28] S. M. Kang'iri and T. Nitta, "A Mathematical Model Predicting Gliding Speed of Actin Molecular Shuttles Over Myosin Motors in the Presence of Defective Motors," in *Bio-Inspired Information and Communications Technologies. BICT 2021.*, vol. 403, T. Nakano, Ed. Cham: Springer International Publishing, 2021, pp. 207–214.

[29] M. J. Greenberg and J. R. Moore, "The molecular basis of frictional loads in the in vitro motility assay with applications to the study of the loaded mechanochemistry of molecular motors," *Cytoskeleton*, vol. 67, no. 5, pp. 273–285, May 2010.

[30] N. M. Bassir Kazeruni, J. B. Rodriguez, G. Saper, and H. Hess, "Microtubule Detachment in Gliding Motility Assays Limits the Performance of Kinesin-Driven Molecular Shuttles," *Langmuir*, vol. 36, no. 27, pp. 7901–7907, Jul. 2020.

[31] L. Scharrel, R. Ma, R. Schneider, F. Jülicher, and S. Diez, "Multimotor transport in a system of active and inactive kinesin-1 motors," *Biophys. J.*, vol. 107, no. 2, pp. 365–372, 2014.

[32] Y. Ishigure and T. Nitta, "Understanding the Guiding of Kinesin/Microtubule-Based Microtransporters in Microfabricated Tracks," *Langmuir*, vol. 30, no. 40, pp. 12089–12096, Oct. 2014.

[33] E. P. Debold, M. A. Turner, J. C. Stout, and S. Walcott, "Phosphate enhances myosin-powered actin filament velocity under acidic conditions in a motility assay," *Am. J. Physiol. - Regul. Integr. Comp. Physiol.*, vol. 300, no. 6, pp. 1401–1408, Jun. 2011.

[34] A. Kishino and T. Yanagida, "Force measurements by micromanipulation of a single actin filament by glass needles," *Nature*, vol. 334, no. 6177, pp. 74–76, Jul. 1988.

[35] D. Riveline *et al.*, "Acting on actin: the electric motility assay," *Eur. Biophys. J.*, vol. 27, no. 4, pp. 403–408, Jun. 1998.

[36] K. Kawaguchi and S. Ishiwata, "Nucleotide-Dependent Single- to Double-Headed Binding of Kinesin," *Science (80-.).*, vol. 291, no. 5504, pp. 667–669, Jan. 2001.

[37] T. Nishizaka, H. Miyata, H. Yoshikawa, S. Ishiwata, and K. Kinosita, "Unbinding force of a single motor molecule of muscle measured using optical tweezers.," *Nature*, vol. 377, no. 6546, pp. 251–4, Sep. 1995.

[38] B. Rupp and F. Nédélec, "Patterns of molecular motors that guide and sort filaments," *Lab Chip*, vol. 12, no. 22, pp. 4903–4910, 2012.

[39] S. Walcott, D. M. Warshaw, and E. P. Debold, "Mechanical coupling between myosin molecules causes differences between ensemble and single-molecule measurements," *Biophys. J.*, vol. 103, no. 3, pp. 501–510, 2012.

[40] C. Leduc *et al.*, "Cooperative extraction of membrane nanotubes by molecular motors," *Proc. Natl. Acad. Sci.*, vol. 101, no. 49, pp. 17096–17101, Dec. 2004.

[41] S. M. Kang'iri, A. Salem, D. V. Nicolau, and T. Nitta, "Effects of defective motors on the active transport in biosensors powered by biomolecular motors," *Biosens. Bioelectron.*, vol. 203, p. 114011, May 2022.

[42] Y. Ishigure and T. Nitta, "Simulating an Actomyosin in Vitro Motility Assay: Toward the Rational Design of Actomyosin-Based Microtransporters," *IEEE Trans. Nanobioscience*, vol. 14, no. 6, pp. 641–648, Sep. 2015.

[43] A. V. Hill, "The heat of shortening and the dynamic constants of muscle," *Proc. R. Soc. London. Ser. B - Biol. Sci.*, vol. 126, no. 843, pp. 136–195, Oct. 1938.